Eur. Phys. J. C (2018) 78:543
https://doi.org/10.1140/epjc/s10052-018-6024-5

THE EUROPEAN PHYSICAL JOURNAL C

Regular Article - Theoretical Physics

New insights on low energy πN scattering amplitudes

Yu-Fei Wang[1], **De-Liang Yao**[2,a], **Han-Qing Zheng**[1,3]

[1] Department of Physics and State Key Laboratory of Nuclear Physics and Technology, Peking University, Beijing 100871, China
[2] Instituto de Física Corpuscular (centro mixto CSIC-UV), Institutos de Investigación de Paterna, Apartado 22085, 46071 Valencia, Spain
[3] Collaborative Innovation Center of Quantum Matter, Beijing 100871, China

Received: 28 March 2018 / Accepted: 23 June 2018 / Published online: 3 July 2018

Abstract The S- and P- wave phase shifts of low-energy pion-nucleon scatterings are analysed using Peking University representation, in which they are decomposed into various terms contributing either from poles or branch cuts. We estimate the left-hand cut contributions with the help of tree-level perturbative amplitudes derived in relativistic baryon chiral perturbation theory up to $\mathcal{O}(p^2)$. It is found that in S_{11} and P_{11} channels, contributions from known resonances and cuts are far from enough to saturate experimental phase shift data – strongly indicating contributions from low lying poles undiscovered before, and we fully explore possible physics behind. On the other side, no serious disagreements are observed in the other channels.

1 Introduction

The pion-nucleon (πN) elastic scattering, as one of the most fundamental and important processes in nuclear or hadron physics, has been studied for decades [1,2]. However, there are still many open questions need to be attained more insights into. For instance, the low energy behavior of the πN elastic scattering amplitude, the pion nucleon σ-term and the relevant intermediate resonances, e.g., $\Delta(1232)$, $N^*(1535)$ and $N^*(1440)$, have attracted sustained attentions, see, e.g., Refs. [3–13]. The $N^*(1535)$ and $N^*(1440)$ are of particular interest. For $N^*(1535)$, the origin of its high mass and its large coupling to the ηN channel have been studied in the literature [14,15]. As for $N^*(1440)$, its quark model interpretation and its coupling to σN channel are still not well understood [16]. Furthermore, it may contain a two-pole structure [17], and the corresponding P_{11} channel may have strange branch cuts in the complex s plane [18]. In this paper, we adopt another approach to study the low energy πN scattering amplitudes. Peking University (PKU) representation [19–23] is a model-independent method based on axiomatic S-matrix arguments. It has been successfully applied to investigate $\pi\pi$ and πK scatterings and, in particular, corroborate the existences of σ and κ resonances [19,21]. The use of PKU representation to study πN scatterings may help us not only to enrich our knowledge of the amplitude structure but also to gain a fresh look at relevant physics in a much more rigorous manner.

The PKU representation factorizes the partial wave two-body elastic scattering S matrix in the form [21]

$$S(s) = \prod_b \frac{1-\mathrm{i}\rho(s)\frac{s}{s-s_L}\sqrt{\frac{s_b-s_L}{s_R-s_b}}}{1+\mathrm{i}\rho(s)\frac{s}{s-s_L}\sqrt{\frac{s_b-s_L}{s_R-s_b}}} \prod_v \frac{1+\mathrm{i}\rho(s)\frac{s}{s-s_L}\sqrt{\frac{s'_v-s_L}{s_R-s'_v}}}{1-\mathrm{i}\rho(s)\frac{s}{s-s_L}\sqrt{\frac{s'_v-s_L}{s_R-s'_v}}} \times \prod_r \frac{M_r^2-s+\mathrm{i}\rho(s)sG_r}{M_r^2-s-\mathrm{i}\rho(s)sG_r} e^{2\mathrm{i}\rho(s)f(s)}, \tag{1}$$

where the functions in resonance terms read

$$M_r^2 = \mathrm{Re}[z_r] + \mathrm{Im}[z_r]\frac{\mathrm{Im}[\sqrt{(z_r-s_R)(z_r-s_L)}]}{\mathrm{Re}[\sqrt{(z_r-s_R)(z_r-s_L)}]}, \tag{2}$$

$$G_r = \frac{\mathrm{Im}[z_r]}{\mathrm{Re}[\sqrt{(z_r-s_R)(z_r-s_L)}]}, \tag{3}$$

and the kinematic factor is defined by

$$\rho(s) = \frac{\sqrt{s-s_L}\sqrt{s-s_R}}{s} \tag{4}$$

with $s_L = (m_1-m_2)^2$ and $s_R = (m_1+m_2)^2$. Here the masses of the two scattering particles are labeled by m_1 and m_2. Furthermore, s_b, s'_v and z_r denote bound state poles (on the real axis below threshold of the first Riemann sheet), virtual state poles (on the real axis below threshold of the second Riemann sheet) and resonances (on the second Riemann sheet off the real axis), respectively. Lastly, the exponential term in Eq. (1) is named as background term since it contains no poles. Actually, the background term carries the information

[a] e-mail: deliang.yao@ific.uv.es

of left-hand cuts (*l.h.c.*s) and right-hand inelastic cut (*r.h.i.c.*) above inelastic thresholds, and it satisfies a dispersion relation,

$$f(s)=\frac{s}{2\pi \mathrm{i}}\int_L ds'\frac{\mathrm{disc}\, f\left(s'\right)}{\left(s'-s\right)s'}+\frac{s}{2\pi \mathrm{i}}\int_{\mathrm{R}'} ds'\frac{\mathrm{disc}\, f\left(s'\right)}{\left(s'-s\right)s'}, \tag{5}$$

where L and R′ denote the *l.h.c.*s and *r.h.i.c.* respectively, and disc stands for the discontinuity of the function $f(s)$ along the cuts. To obtain the background function $f(s)$ in Eq. (5), a first-order subtraction has been performed at the point $s_0=0$, at which the subtraction constant term $f(s_0)$ vanishes, i.e. $f(0)=0$, as pointed out in Ref. [23]. It should be emphasized that resonances other than the second sheet ones are not presented in the resonance terms in Eq. (1), rather, their contributions are hidden in the *r.h.i.c.* integral of Eq. (5) [23].

PKU representation is derived based on first principles of S-matrix theory, thus, in principle it is rigorous and universal for two-body elastic scatterings.[1] Besides, the production representation equipped itself with additive phase shifts stemming from different contributions, which makes the analysis of phase shifts clear and convenient, and enables one even to find out hidden contributions. The phase shifts given by PKU representation are sensitive to (not too) distant poles, letting one determine pole positions rather accurately. Moreover, each phase shift contribution has a definite sign: bound states always give negative contributions, while virtual states and resonances always give positive contributions.[2] Furthermore, the *l.h.c.*s would give negative phase shifts.[3] The observation that the *l.h.c.*s give a large and negative contribution is crucial to firmly establish the very existence of the σ meson ($f_0(500)$) in Ref. [19], and the κ resonance ($K^*(800)$) in Ref. [21]. The essence of PKU representation is not to directly unitarize the amplitude itself, rather, it unitarizes the *l.h.c.*s of the perturbative amplitude and hence hazardous spurious poles can be avoided. Specific example concerning the advantage of PKU representation, compared to some conventional unitarization approaches (like Padé approximation), can be found in Ref. [27].

In this paper, PKU representation is employed to study the S- and P- wave channels of the πN elastic scattering. On the one hand, the various relevant poles are incorporated as inputs or determined by fit. On the other hand, the contribution of *l.h.c.*s is deduced with the help of chiral perturbative amplitudes of $\mathcal{O}(p^2)$ at tree level, derived in a relativistic baryon chiral perturbation theory (BChPT) [28]. In the following Sect. 2, the basic formulae relevant to the calculation are shown. In Sect. 3 the numerical results are presented and discussed. Finally Sect. 4 contains conclusions and outlook of this paper. The tree amplitudes up to $\mathcal{O}(p^2)$ and their partial-wave projection are relegated to Appendices A and B, respectively. The major uncertainties of the estimation of the background integral are compiled in Appendix C. Finally, a comparison between the perturbative result and the subthreshold expansion from Ref. [13] in P_{11} channel is demonstrated in Appendix D.

2 Theoretical framework

2.1 Left-hand cut contributions implied by BChPT at tree-level

In the $SU(2)$ isospin limit, the πN Lagrangians relevant to the calculation up to $\mathcal{O}(p^2)$ are [29]:

$$\mathcal{L}^{(1)}_{\pi N}=\bar{N}\left(\mathrm{i}\not{D}-M+\frac{1}{2}g\not{u}\gamma^5\right)N, \tag{6}$$

$$\begin{aligned}\mathcal{L}^{(2)}_{\pi N}=&c_1\langle\chi_+\rangle\bar{N}N-\frac{c_2}{4M^2}\langle u^\mu u^\nu\rangle(\bar{N}D_\mu D_\nu N+\mathrm{h.c.})\\&+\frac{c_3}{2}\langle u^\mu u_\mu\rangle\bar{N}N-\frac{c_4}{4}\bar{N}\gamma^\mu\gamma^\nu\left[u_\mu,u_\nu\right]N,\end{aligned} \tag{7}$$

with M being the mass of the nucleon, g being the axial current coupling constant and $c_i(i=1,2,3,4)$ the $\mathcal{O}(p^2)$ coupling constants. The "$\langle\cdots\rangle$" denotes the matrix tracing in isospin space. The pion fields are compiled in

$$u(x)=\exp\left(\frac{\mathrm{i}\pi^a\tau^a}{2F}\right), \tag{8}$$

with F being the pion decay constant in the chiral limit and τ^a standing for Pauli matrices. The chiral building blocks in Eqs. (6) and (7) are as follows:

$$\begin{aligned}D_\mu&=\partial_\mu+\Gamma_\mu,\\ \Gamma_\mu&=\frac{1}{2}\left[u^\dagger(\partial_\mu-\mathrm{i}r_\mu)u+u(\partial_\mu-\mathrm{i}l_\mu)u^\dagger\right],\\ u_\mu&=\mathrm{i}\left[u^\dagger(\partial_\mu-\mathrm{i}r_\mu)u-u(\partial_\mu-\mathrm{i}l_\mu)u^\dagger\right],\\ \chi_+&=u^\dagger\chi u^\dagger+u\chi^\dagger u,\\ \chi&=2B_0(s+ip),\end{aligned}$$

During the procedure of calculation one needs to set $2B_0s\to 2B_0m_q\equiv m^2$ with m being the pion mass, while the other sources (l_μ, r_μ and p) are switched off. To obtain the amplitudes with definite isospin I and angular momentum J, one

[1] It is only confined to the situation of elastic scatterings. For coupled channel situation, a production representation is not established, see Ref. [24].

[2] Actually, the PKU representation method is the quantum field theory correspondence of Ning Hu representation in quantum mechanical scattering theory, see Ref. [25].

[3] This lacks of rigorous mathematical prove, but is correct empirically, and is to be discussed later at tree level. There exists a corresponding prove at the level of quantum mechanical scattering theory under some assumptions, see Ref. [26].

should decompose the isospin structure and then perform partial wave projection. For isospin decomposition,

$$T(\pi^a + N_\mathrm{i} \to \pi^{a'} + N_\mathrm{f}) = \chi_\mathrm{f}^\dagger \left(\delta^{a'a} T^S + \frac{1}{2}[\tau^{a'}, \tau^a] T^A \right) \chi_\mathrm{i}, \tag{9}$$

where χ_i and χ_f are isospinors of initial and final nucleon states, respectively. Then the amplitudes with isospins $I = \frac{1}{2}, \frac{3}{2}$ can be written as

$$T^{I=1/2} = T^S + 2T^A, \tag{10}$$
$$T^{I=3/2} = T^S - T^A. \tag{11}$$

Further, the Lorentz structure of the above isospin amplitudes reads

$$T^I = \bar{u}(p', s') \Big[A^I(s,t) + \frac{1}{2}(\not{q} + \not{q}') B^I(s,t) \Big] u(p,s), \tag{12}$$

where s, t are Mandelstam variables, and q and q' are the 4-momenta of initial and final states of pions, respectively. The tree-level A^I and B^I up to $\mathcal{O}(p^2)$ are listed in Appendix. A. The helicity amplitudes in the centre of mass frame can be expressed in terms of functions A^I and B^I as

$$\begin{aligned} T^I_{++} =& (\frac{1+z_s}{2})^{\frac{1}{2}} [2MA^I(s,t) + (s - m^2 - M^2) B^I(s,t)], \\ T^I_{+-} =& -(\frac{1-z_s}{2})^{\frac{1}{2}} s^{-\frac{1}{2}} [(s - m^2 + M^2) A^I(s,t) \\ & + M(s + m^2 - M^2) B^I(s,t)], \end{aligned} \tag{13}$$

where the subscripts "±" are abbreviations of helicity $h = \pm 1/2$. Moreover, the first and second subscripts correspond to the helicities of the initial and final nucleon states, respectively. z_s is defined as the cosine of the scattering angle. The partial wave projection formulae are given by

$$\begin{aligned} T^{I,J}_{++} &= \frac{1}{32\pi} \int_{-1}^{1} dz_s T^I_{++}(s, t(s,z_s)) d^J_{-1/2,-1/2}(z_s), \\ T^{I,J}_{+-} &= \frac{1}{32\pi} \int_{-1}^{1} dz_s T^I_{+-}(s, t(s,z_s)) d^J_{1/2,-1/2}(z_s), \end{aligned} \tag{14}$$

with d^J to be the Wigner D-matrix. To be specific, the six S- and P- wave amplitudes (in $L_{2I\,2J}$ convention) can be represented in terms of helicity amplitudes as follows:

$$\begin{aligned} T(S_{11}) &= T^{1/2,1/2}_{++} + T^{1/2,1/2}_{+-}, \\ T(S_{31}) &= T^{3/2,1/2}_{++} + T^{3/2,1/2}_{+-}, \\ T(P_{11}) &= T^{1/2,1/2}_{++} - T^{1/2,1/2}_{+-}, \\ T(P_{31}) &= T^{3/2,1/2}_{++} - T^{3/2,1/2}_{+-}, \\ T(P_{13}) &= T^{1/2,3/2}_{++} + T^{1/2,3/2}_{+-}, \\ T(P_{33}) &= T^{3/2,3/2}_{++} + T^{3/2,3/2}_{+-}. \end{aligned} \tag{15}$$

The explicit expressions of the partial-wave helicity amplitudes can be found in Appendix B. From Eq. (15) the symmetry proposed by MacDowell in Ref. [30] is manifest: if the $s^{-1/2}$ factor in T_{+-} changes its sign while other terms remain fixed, then the S- wave amplitudes are transformed into the corresponding P-wave ones. That property is automatically fulfilled in perturbation theory, hence also satisfied here since we use perturbative amplitudes to evaluate the left-hand cut integrals. Eventually, the discontinuity of function f can be deduced through (the symbols of the channels are omitted)

$$\begin{aligned} \mathrm{disc}\big[f(s)\big] &= \mathrm{disc}\left[\frac{\ln S(s)}{2i\rho(s)}\right], \\ S(s) &= 1 + 2i\rho(s)T(s), \end{aligned} \tag{16}$$

where $T(s)$ is perturbatively calculated here, and function $f(s)$ can be obtained by using Eq. (5). At tree level, the left-hand cut structure for T is quite simple: a kinematic cut $(-\infty, 0]$ and a segment cut $[(M^2 - m^2)^2/M^2, 2m^2 + M^2]$ due to the u-channel nucleon exchange. Note that $\rho(s)$ has an extra branch-cut $(-\infty, (M-m)^2]$ by definition in Eq. (4), so the cuts of $S(s)$ should be $(-\infty, (M-m)^2]$ and $[(M^2 - m^2)^2/M^2, 2m^2 + M^2]$,[4] thus the background function is

$$\begin{aligned} f(s) = & -\frac{s}{\pi} \int_{s_c}^{(M-m)^2} \frac{\ln|S(w)| dw}{2\rho(w) w (w-s)} \\ & + \frac{s}{\pi} \int_{(M^2-m^2)^2/M^2}^{2m^2+M^2} \frac{\mathrm{Arg}[S(w)] dw}{2iw\rho(w)(w-s)}. \end{aligned} \tag{17}$$

From Eq. (17) it is found that the dispersion integral contains a logarithmic term and once subtraction,[5] which significantly suppresses the bad behavior of perturbation theory in high energy region – even if the integral domain of the first term is chosen to be $(-\infty, (M-m)^2]$, the integral still converges. That property guarantees the results to be insensitive to high energy contributions. However, perturbative calculations would inevitably become invalid when w is too large, so one has to assign the integral domain a cut-off parameter s_c. In principle the exact value of s_c is unknown, and may be fixed by fitting to the data if one tentatively regards Eq. 17 as a parameterization of the left-hand cut. On the other side, it is also educative to chose s_c to be at the boundary of perturbation theory convergence region, in order to evaluate

[4] The full analytic structure of the *l.h.c.*s can be found in Ref. [31]. At $\mathcal{O}(p^2)$ level, there is no circular cut.

[5] Note that even though due to the $s^{-1/2}$ factor, the limits for $T(s)$ when $s \to 0^{\pm}$ do not equal, from Appendix B it is found that each channel satisfies $T(s \to 0) \sim s^{-c}$ for constant c, which leads to the result $f(0) = 0$ as proposed in Ref. [23].

Table 1 Intermediate poles added in each channel

Channels	$I\left(J^P\right)$	Poles
S_{11}	$\frac{1}{2}\left(\frac{1}{2}^-\right)$	$N^*(1535)$, $N^*(1650)$, $N^*(1895)$
S_{31}	$\frac{3}{2}\left(\frac{1}{2}^-\right)$	$\Delta(1620)$, $\Delta(1900)$
P_{11}	$\frac{1}{2}\left(\frac{1}{2}^+\right)$	N, $N^*(1440)$, $N^*(1710)$, $N^*(1880)$
P_{31}	$\frac{3}{2}\left(\frac{1}{2}^+\right)$	$\Delta(1910)$
P_{13}	$\frac{1}{2}\left(\frac{3}{2}^+\right)$	$N^*(1720)$, $N^*(1900)$
P_{33}	$\frac{3}{2}\left(\frac{3}{2}^+\right)$	$\Delta(1232)$, $\Delta(1600)$, $\Delta(1920)$

the contributions from where perturbation theory is valid. Of course, meaningful physical outputs should be immune from such an ambiguity of the left-hand cut integral.

Actually the contribution from the u-channel cut is numerically very small,[6] hence the dominant contribution is from the first term of Eq. (17), which is always negative in physical region ($s > (M+m)^2$), since $\rho(w)w(w-s) > 0$ when $w < (M-m)^2$ and $|S| > 1$ in perturbation theory. Besides, the *r.h.i.c.* is not considered for the moment, since the energy region to be analyzed (from the πN threshold to 1.16 GeV) is below the inelastic threshold, where the *r.h.i.c.* contribution is empirically small. However, this topic is to be discussed further in Sect. 3.3.

2.2 Known-pole contributions estimated from experiments

The above discussions are devoted to the estimation of the cut contributions from chiral perturbative amplitudes. In practice, one also needs to take into account the pole contributions. The known poles (nucleon bound state and above-threshold resonances), listed in Table 1 [32], are under our consideration.

However, the PKU method can only deal with poles on the first and second Riemann sheets, namely, the poles located on the third Riemann sheet given by experiments

$$\sqrt{s}^{\rm III} = M_{\rm pole} - \frac{i}{2}\left(\Gamma_{\rm inelastic} + \Gamma_{\pi N}\right)$$

cannot be used directly.[7] Under narrow width approximation, the second sheet poles (usually called shadow poles) may be estimated by

$$\sqrt{s}^{\rm II} = M_{\rm pole} - \frac{i}{2}\left(\Gamma_{\rm inelastic} - \Gamma_{\pi N}\right). \tag{18}$$

[6] This is due to that the near threshold u channel exchange $1/(u-M^2)$ can be approximately represented as a contact interaction, which leaves no left-hand cut at all.

[7] The information of the poles on third or higher sheets is hidden in the inelastic cut in Eq. (5) and their contributions are rather indirect [23].

With the preparations made in this section, we proceed with the numerical study in the next section.

3 Numerical results and discussions

3.1 Prelude: a K-matrix fit and spurious poles

Here we use K-matrix method to determine the coupling constants c_i. The influence of different choices of c_i parameters is mild as discussed in Appendix. C.1. In our numerical computation, values of the masses and $\mathcal{O}(p^1)$ coupling constants, see Eq. (6), are taken from Ref. [33]: $M = 0.9383$ GeV, $m = 0.1396$ GeV, $F = 0.0924$ GeV and $g = 1.267$. A K-matrix fit is performed to the data of S_{11}, S_{31}, P_{11}, P_{31} and P_{13} channels[8] provided by George Washington University (GWU) group [35]. Unfortunately, the uncertainties of data are not provided by GWU group. Therefore, we assign errors to the data in the same way as done in Ref. [5]:[9]

$$\Delta_i = \sqrt{e_s^2 + e_r^2\delta_i^2}\,, \tag{19}$$

where Δ_i is the total error of the phase shift δ_i, while the systematic error is assigned as $e_s \sim 0.1^\circ$ and for relative statistical error $e_r \sim 2\%$. The tree-level K-matrix formula is

$$\begin{aligned} T_K &= \frac{T}{1 - i\rho\, T}\,, \\ \delta_K &= \arctan\left[\rho\, T\right]. \end{aligned} \tag{20}$$

We fit 20 data points (corresponding to $W \equiv \sqrt{s} \in [1.0776, 1.1600]$ GeV) in each channel. The fitted values of parameters are

$$\begin{aligned} &c_1 = -0.841\ \text{GeV}^{-1},\ c_2 = 1.170\ \text{GeV}^{-1}, \\ &c_3 = -2.618\ \text{GeV}^{-1},\ c_4 = 1.677\ \text{GeV}^{-1}\,, \end{aligned} \tag{21}$$

with the fit quality $\chi^2/\text{d.o.f} = 1.850$. The fit results are plotted in Fig. 1.

Since K-matrix method gives the unitarized amplitudes (see Eq. (20)), it seems that poles can also be extracted. For instance, in S_{11} channel, the poles given by K-matrix are listed in Table. 2.

Firstly we discover that the K-matrix gives a near-threshold resonance locating at $0.954 - 0.265i$ GeV, but the

[8] The P_{33} channel cannot fit to the data well at tree level without explicit $\Delta(1232)$ field, hence is excluded.

[9] Actually, a more adequate way is to use the phase shifts data (with errors) generated by the recent Roy–Steiner-equation analysis of the πN scattering [13], as was done in Ref. [12]. This alternative will be adopted in the future work of PKU-representation analysis at $\mathcal{O}(p^3)$ level [38] , aiming at a more precise justification of the somewhat qualitative conclusions in this paper.

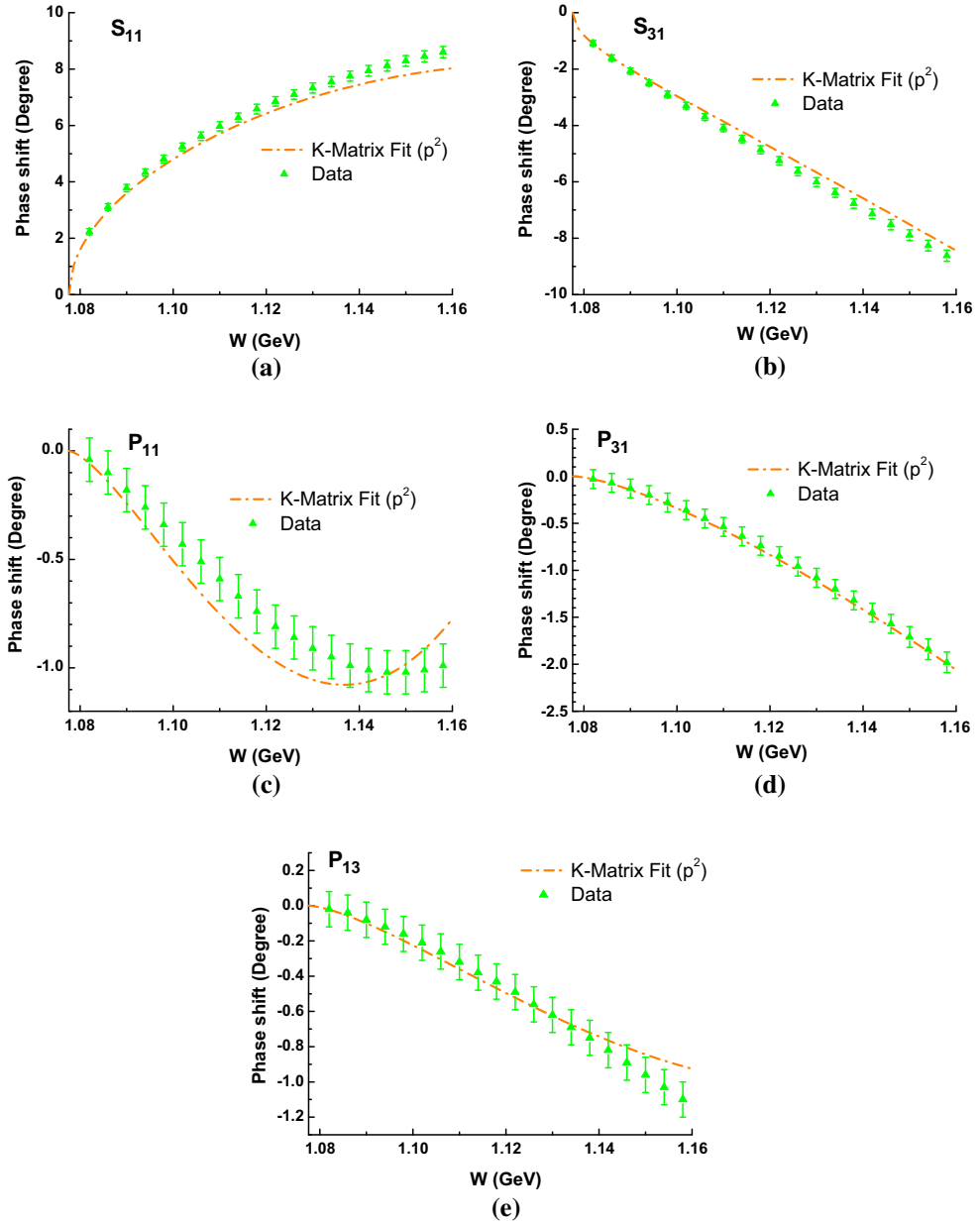

Fig. 1 $\mathcal{O}(p^2)$ K-matrix fit results of five channels

Table 2 The pole positions given by K-matrix method of S_{11} channel

Resonances (GeV)	Spurious poles (GeV)
$0.954 - 0.265i$	$0.733 + 0.089i$
$2.254 - 0.067i$	$1.431 + 0.253i$

K-matrix also generates some poles on the first sheet off the real axis, which are called spurious poles,[10] and have already been discussed in Ref. [21]. Those poles violate causality and hence are not allowed. Due to the existence of nearby spurious poles, the other poles given by K-matrix become unauthentic. If one uses PKU representation to separate the contributions in K-matrix, it is found that the "good" description of data rooted in the cancellation between large contributions from resonances and spurious poles, leaving a vigorously suppressed left-hand cut contribution, see Fig. 2.

In fact K-matrix amplitude in other channels may behave even worse. For example, in S_{31} channel the K-matrix amplitude generates two bound states as well as two spurious poles, see Table. 3.

[10] The spurious poles satisfy the equation $1 - i\rho T = 0$, and always give negative phase shifts in the convention of PKU representation.

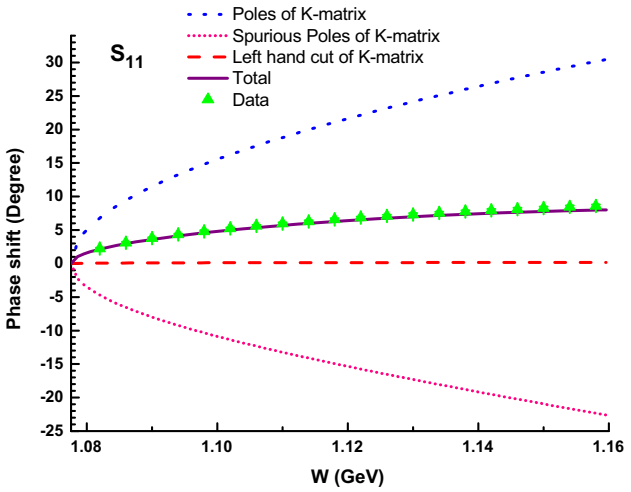

Fig. 2 PKU representation of the phase shift of S_{11} channel based on K-matrix fit

Table 3 The pole positions given by K-matrix method of S_{31} channel

Bound states (GeV)	Spurious poles (GeV)	Resonances (GeV)
0.959	$0.647 + 0.064i$	$0.784 - 0.215i$
0.916	$1.150 + 0.317i$	$0.938 - 0.0006i$
		$1.626 - 0.142i$

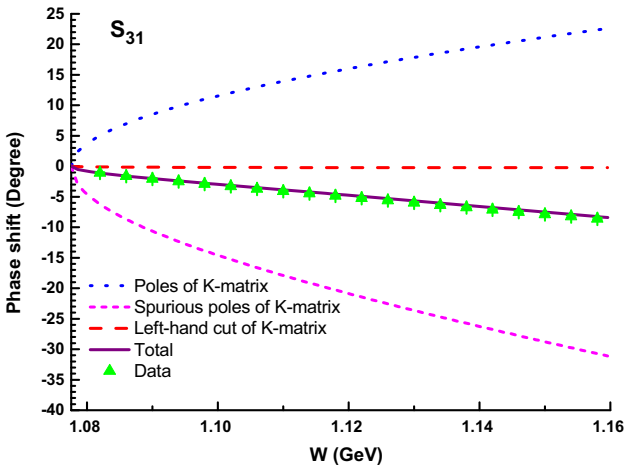

Fig. 3 PKU representation of the phase shift of S_{31} channel based on K-matrix fit

The PKU representation analyses of the K-matrix amplitude in S_{31} channel is plotted in Fig. 3.

In fact, the K-matrix method is constructed only relying on the right-hand unitarity, while PKU representation is more sophisticated since both analyticity and unitarity are maintained. From statements above, it is clear that the K-matrix approach is not at all admirable in determining distant poles, though we use it as a rough approximation to extract the $\mathcal{O}(p^2)$ coefficients. Therefore, it is pleasurable to use the strategy of PKU representation proposed in Refs. [19,21–23] to tackle the spurious-pole problem.

3.2 Pertinent PKU representation of phase shifts

To apply PKU representation, one needs a value of the cut-off parameter s_c. As discussed before, we at first assess its value from the region where perturbation calculation works. That region can be obtained via different methods, e.g. through the unitarity bound (see Figure 14 in Ref. [9]), or by assuming the validity of perturbation calculation till meeting the first resonance pole. Here we use the shadow pole location of $N^*(1440)$, which is the first resonance related to complicated couple-channel dynamics.[11] Since the chiral expansion is at the point $s = u = M^2 + m^2$, $t = 0$, we set the distance between $M^2 + m^2$ and $N^*(1440)$ shadow pole location as the convergence radius r, and hence the cut-off on the left-hand cut is at $s_c = M^2 + m^2 - r \simeq -0.08$ GeV^2. In what follows, actually, it is seen that this choice of s_c is reasonable in most channels; even if in quantitative analyses of P_{11} channel the cut-off parameter should be tuned, the major physical outputs and conclusions are insensitive to its value.

The contributions from known poles and *l.h.c.*s to the phase shift in the S- and P- wave[12] channels are plotted in Fig. 4, within the scheme of PKU representation.

From Fig. 4, firstly we observe significant contributions from well established poles: in P_{11} channel the nucleon itself serves as a bound state of the πN system, generating a large and negative phase shift, while in P_{33} channel the $\Delta(1232)$ resonance gives a large positive contribution. Secondly, the background terms usually contribute sizable and negative phase shifts as expected. Surprisingly, it is found that there exist huge disagreements between the phase shifts from known poles plus cut and the data, especially in S_{11} and P_{11} channels. Therein the results of known poles plus cut have missed some important positive contributions.

One may find that in other channels discrepancies also exist, but are less significant. The discrepancies in P_{13} and P_{33} channels indicate that these channels need a slightly larger s_c parameter; the S_{31} channel may require fine-tuning of s_c parameter and higher order corrections (of the *l.h.c.*); while in P_{31} channel the discrepancy is a bit larger – an s_c closer to $(M + m)^2$, higher order perturbation calculation or

[11] In principle a complete calculation of the *l.h.c.*s should contain $\Delta(1232)$ as a genuine state, but the *l.h.c.* contribution from t and u channel $\Delta(1232)$ exchange is ignorable.

[12] In order to separate the contributions clearly, here we do not use free parameters to constraint the near-threshold behavior ($\delta(s) \sim \mathcal{O}(k^3)$) of the P- wave amplitudes. As can be seen in Fig. 4, the near-threshold condition can not be satisfied automatically due to the absence of some hidden contributions and the uncertainties in evaluating the *l.h.c.*s.

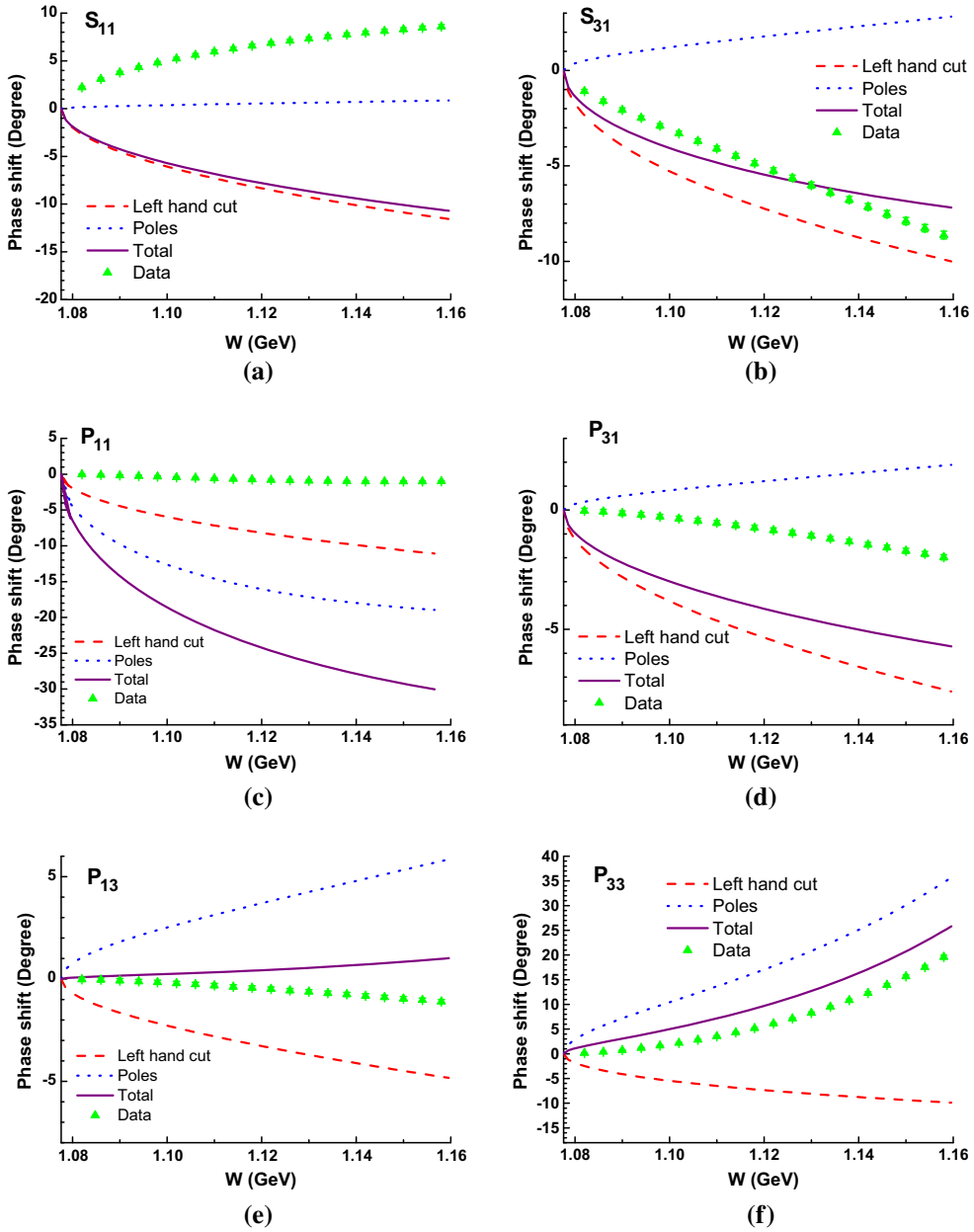

Fig. 4 Tree level PKU representation analyses of the πN elastic scattering in s and p waves

other contributions may be needed. Moreover, changing the c_i parameters may have some impact on those channels. One refers to Appendix. C.1 and C.2 for the different choices of c_i and the cut-off parameters. All in all, the discrepancies in those four channels are at quantitative level and may be ascribed to some details of dynamics. On the contrary, the discrepancies in S_{11} and P_{11} channels are qualitatively severe and can never be remedied through such tricks: only when some extra large and positive contributions intrude would they disappear.

There could be some possible interpretations of the huge discrepancies in the S_{11} and P_{11} channels: firstly it is natural to suspect that the one-loop contributions in those two channels may be crucial; secondly, other branch cuts which are not included in the discussions above may be non-ignorable, e.g. the *r.h.i.c.* and the type of cut proposed by Ref. [18]; thirdly, the previous calculation of the shadow poles is carried out under a rough approximation, while the actual shadow pole positions may be very different from what the approximation gives; finally, we can not exclude the existence of some hidden poles, e.g. virtual states, resonances below the threshold, resonances with extremely large widths, or two-pole structures [17], which cannot be observed directly by the experiments.

As for the first interpretation above, we believe that the higher order contributions of BChPT may have some significance numerically, but they are very unlikely to distort the results totally. As already mentioned before, the background function in Eq. (5) is of logarithmic form and once-subtracted, which would make the function insensitive to the higher order terms. This is also a lesson we learned from $\pi\pi$ scatterings in Ref. [22]. One refers to Appendix. C.3 for the assessment of the dependence of the results on the order of chiral expansion at $\mathcal{O}(p^1)$ and $\mathcal{O}(p^2)$ level. We also extend our calculation of the *l.h.c.* to the $\mathcal{O}(p^3)$ level in S_{11} channel. The result confirms our speculation that the high order corrections to the *l.h.c.* are not qualitatively important. The other interpretations will be discussed in the following two subsections.

3.3 Estimation of the right-hand inelastic cut

The contribution from *r.h.i.c.* is expected to be less significant below the inelastic threshold. Actually, analogous to Eq. (17), the contribution from the *r.h.i.c.* can be estimated by

$$f_{\mathrm{R}'}(s) = \frac{s}{\pi}\int_{(2m+M)^2}^{\Lambda_R^2} \frac{\sigma_R(w)dw}{w(w-s)}, \qquad \sigma_R(w) = -\left\{\frac{\ln[\eta(w)]}{2\rho(w)}\right\}, \tag{22}$$

where $0 \leq \eta \leq 1$ represents the inelasticity of πN scatterings above the inelastic threshold, i.e. the $\pi\pi N$ threshold $(2m+M)^2$, and the cut-off parameter of the integral in Eq. (22) is denoted as Λ_R. Equation (22) indicates that the *r.h.i.c.* contribution is positive definite. In the following computation, the inelasticity function $\eta(s)$ is taken from Ref. [35]. As for the cut-off Λ_R, the energy region of the data is only up to 2.48 GeV, but in P_{11} channel the inelasticity is still near 0.1 when the centre of mass energy reaches 2.48 GeV. Hence to avoid the disappreciation of right-hand cut contribution, we take a cut-off of $\Lambda_R = 4.00$ GeV and employ an extrapolation of the data to 4.00 GeV to estimate the function $f_{\mathrm{R}'}$ in Eq. (22). The phase shifts from inelastic cuts of different channels are plotted in Fig. 5.

It is clear to see that in P_{11} channel the *r.h.i.c.* contributes sizeably to the phase shift (about 8 degrees at $\sqrt{s} = 1.16$ GeV), but this is still far from enough to compensate the discrepancy (nearly 32 degrees at $\sqrt{s} = 1.16$ GeV); meanwhile, the phase shifts from *r.h.i.c.* in other channels are much smaller, thus the discrepancy of S_{11} channel can neither be interpreted by it.

Besides, to investigate other possible hidden cut structures (as suggested by Ref. [18]) goes beyond the scope of present paper.

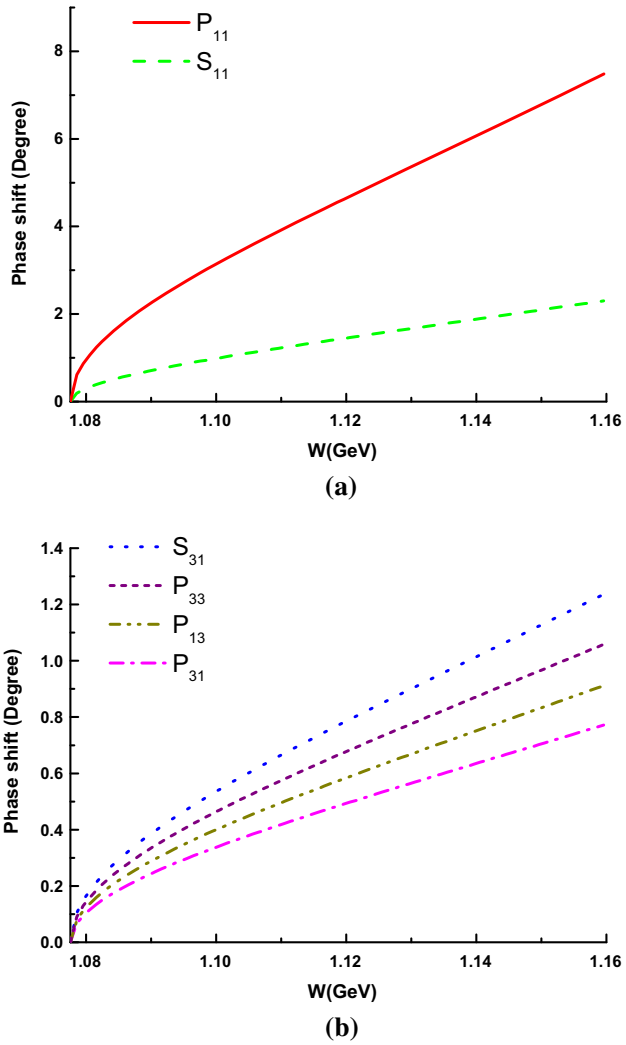

Fig. 5 The phase shifts from *r.h.i.c.*

3.4 Hidden pole analyses: P_{11} channel

After all the discussions above, it seems that the existence of hidden poles is the last remaining interpretation. It is noticed that we can not tell the differences between shadow pole positions very different from Eq. (18) and extra hidden poles, because shadow pole positions determined by Eq. (18) contributes little to the phase shifts at low energies;[13] however, the missing positive contributions in S_{11} and P_{11} channels are too large to be filled by shadow pole positions close to what Eq. (18) gives, so it is more natural to believe that the discrepancy stems from extra hidden poles, which are discussed as follows.

We proceed by keeping the known poles and the inelastic cut, meanwhile we still keep the values of c_i coefficients in

[13] This argument also indicates that the two-pole structures under Eq. 18 cannot explain the discrepancy.

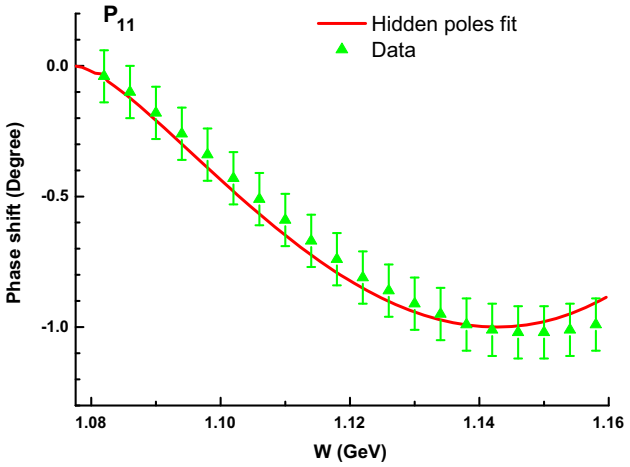

Fig. 6 The phase shift results with extra virtual states in P_{11} channel

Eq. (21). Threshold P- wave behavior is used as a constraint: the phase shift cannot contain $\mathcal{O}(k^1)$ term (here k is the 3-momentum of the πN system in center of mass frame). It is found that if we set the extra pole to be one resonance and perform a fit to the data, it always automatically runs to the real axis and become two virtual poles: one survives while the other falls to the pseudo-threshold ($\sqrt{s} = M - m$) and vanishes. The P_{11} data requires passionately one single virtual state near the πN threshold. Notice that both the resonance pole and the virtual pole give similar positive phase shift, it is amazing that the fit using PKU representation can easily distinguish the two very similar contributions. This is very remarkable – as will be revealed later, that a single nearby virtual state is actually what is needed physically. It is found that in P_{11} channel a good fit requires a much larger s_c than $-0.08\,\text{GeV}^2$, but a nearby virtual state always exists irrespective of the choice of the cut-off parameter.[14] Figure 6 affords an example with $\chi^2_{P_{11}}/\text{d.o.f} = 0.201$, where the virtual pole locates at 980 MeV (with statistical error 0.496 MeV). Note that the unnaturally small value of the χ^2/d.o.f, here and in the next subsection, is a warning that the error estimation budget specified in Eq. (19) is rather rough.

In the following we show that through investigating the amplitude, the existence of that pole is found to be quite reasonable – actually, it is just a kinematic companionate pole of the nucleon bound state. In the vicinity of the nucleon bound state pole, the S matrix takes the form

$$S(s) \sim \frac{r_0}{s - M^2} + b_0 + \mathcal{O}(s - M^2)$$

where $r_0 \in \mathbb{R}$ is the residue and the constant b_0 represents the background. The dominant term $r_0/(s - M^2)$ is a typical hyperbola with the horizontal axis being one of its asymptotes, while arbitrary non-zero real b_0 would lead the function to generate a zero on the first Riemann sheet, which, according to the rule of analytic continuation $S^{\text{II}} = 1/S^{\text{I}}$, indicates the existence of a virtual state pole on the second sheet.[15] Such a simple explanation on the necessity of a nearby virtual state, is firstly revealed here, to the best of our knowledge. For example, in Ref. [4], a somewhat arbitrary CDD pole is introduced to take the role of such a virtual state without further investigation of its origin.

Of course a bound state does not always induce a nearby virtual state (a famous example is the deuteron), but here the nucleon pole is an "elementary" state and is already contained in the perturbative amplitude, which is totally different from a molecular bound state generated from some non-perturbative re-summation. We think this mechanism of kinematical partner should be rather general for non-molecular bound states. Actually we believe an "elementary" bound state must have a nearby companion regardless of the dynamical details, at least in the weak coupling situation. Our statement can actually be related to the result given in Ref. [36] at least in S-wave. For P- wave, even a molecular bound state is associated with a virtual companion as revealed by potential scattering theory (see for example Ref. [37]).

To proceed, the partial-wave S matrix given by perturbative calculation also suggests a zero at

$$\left[M^2 + \frac{2g^2m^3M}{3F^2\pi} - \frac{g^2m^6(3 + 4g^2 - 4c_3M + 8c_4M)}{18F^4\pi^2} + \cdots\right]^{1/2} \sim 976\ \text{MeV}, \tag{23}$$

see Fig. 7, which is, as it should be, close to the result 980 MeV given by the fit of PKU representation with the P- wave constraint in Fig. 6.[16]

In addition, one can also use the subthreshold expansion with the constants given by Roy-Steiner equations in Ref. [13] to verify the existence of such a zero, see Appendix. D.

In order to further examine the importance of such a virtual state, we calculate its residue r_v in S matrix on the second Riemann sheet as follows:

$$r_v = \lim_{s \to s_v} \frac{s - s_v}{S(s)} = 0.046\ \text{GeV}^2; \tag{24}$$

here $S(s)$ is the complete S matrix of P_{11} channel including the hidden virtual state (at $\sqrt{s_v} = 980$ MeV) determined by

[14] When $s_c = -0.08\ \text{GeV}^2$, the fit quality is poor, but the P-wave constraint gives a virtual state at 944 MeV, which is above the nucleon pole and not far from the location when $s_c = -9\,\text{GeV}^2$, which generates Fig. 6.

[15] Exactly speaking, b_0 is complex due to the existence of the u-channel nucleon exchange. Nevertheless, since the u-channel cut is numerically very small, the main conclusion of the observation here remains unchanged.

[16] A perturbative study at $\mathcal{O}(p^3)$ level shows that the S matrix zero is at 978 MeV, so it is very stable against the chiral expansion.

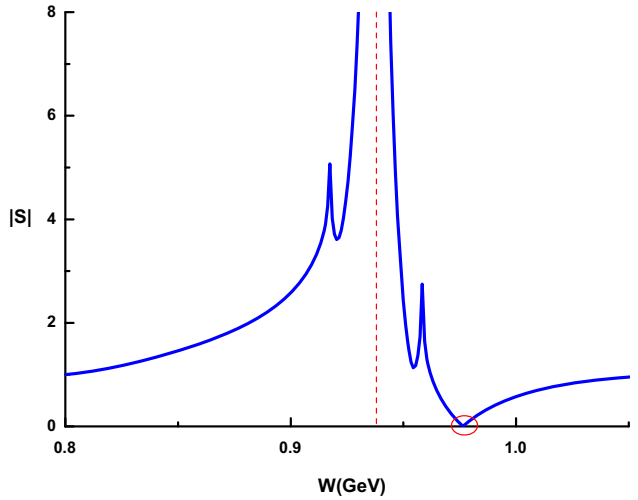

Fig. 7 The absolute value of perturbative calculated S matrix in P_{11} channel below threshold. The vertical red dashed line marks the position of the nucleon bound state pole, and the red circle illustrates the zero of the S matrix. The two spikes correspond to the two branch points of the u-channel cut

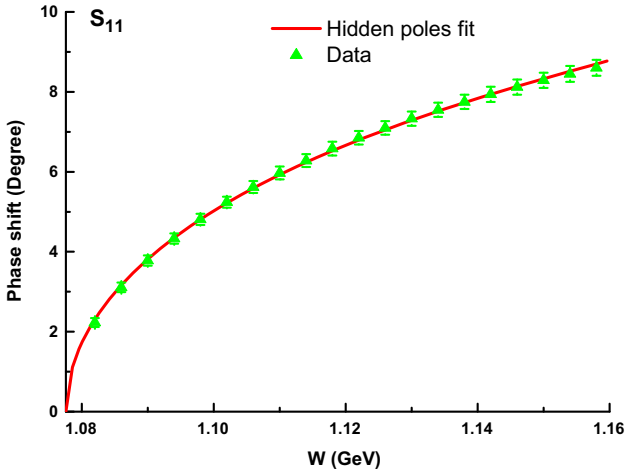

Fig. 8 The hidden pole fit to data in S_{11} channel. The background contribution can be read off from Fig. 4a. The "crazy resonance" saturates the gap between the data and the background contribution

fit. The residue of the nucleon pole (r_N) is also calculated as a control:

$$r_N = \lim_{s\to M^2}(s-M^2)S(s) = -0.146\ \text{GeV}^2, \tag{25}$$

which is approximately three times as large as that of the virtual state (to be compared with perturbative result $r_N = -0.114\ \text{GeV}^2$). Whereas the virtual state is closer to the threshold than the nucleon, its residue cannot be regarded ignorable compared to the nucleon pole.

Furthermore, it is found that the virtual state plays a crucial role in determining the sign of the residue at nucleon pole. From the analytical expressions in Eq. (1), one can easily verify it with some primary algebra that all the terms contribute to the residue of the nucleon pole positively (notice that in the present scheme different contributions to the residue are productive), except for virtual states lying above the nucleon pole. In other words, to reproduce the negative residue at nucleon pole, i.e., $\propto i\rho(M^2)g_{\pi N}^2 < 0$, a virtual state as discovered in this paper is essential.

The above analysis demonstrates that the PKU representation is very sensitive to the low lying pole positions and hence is very powerful and reliable in pinning down the correct low-energy pole positions, which encourages us to find out the hidden contribution in S_{11} channel similarly.

3.5 Hidden pole analyses: S_{11} channel

For S_{11} channel, we keep Eq. (18) as a solution for $N^*(1535)$ shadow pole position, and add one more resonance with mass and width as free parameters, meanwhile we keep $s_c = -0.08\ \text{GeV}^2$. Unlike P_{11} channel, our fit leads to a resonance pole lying below the πN threshold: $\sqrt{s}^{\text{II}} = 0.808 - 0.055i$ GeV, with the fit quality $\chi^2_{S_{11}}/\text{d.o.f} = 0.109$ (see Fig. 8), and its residue of S can be calculated in the same way as Eq. (24), resulting in $(0.422+0.107i)^2\ \text{GeV}^2$. Notice that this pole location may not be that accurate even though we have little doubt on the very existence of such a pole. The dependence of the pole location on the variation of background contribution is analyzed in Appendix. C.2. For example, taking $s_c = -\infty$, one gets $\sqrt{s}^{\text{II}} = 0.914 - 0.205i$ GeV, which still locates well below threshold, with a similar fit quality $\chi^2_{S_{11}}/\text{d.o.f} = 0.018$. From these analyses, we see that the vast change of cut-off parameter does not lead to a significant change of the pole position. From Table. 4 we roughly estimate the pole location to be[17]

$$\sqrt{s}^{\text{II}} = (0.861 \pm 0.053) - (0.130 \pm 0.075)i\ \text{GeV}. \tag{26}$$

At current stage, we think it is very difficult to further pin down the uncertainty of the imaginary part of the S_{11} pole. In principle, one can use some models (like resonance exchange models or Regge model) to evaluate the left-hand cut contributions in high energy region, and this is left for future investigation.

The hidden resonance found above is beyond direct experimental observations and is difficult to understand. However, we would try to give it a reasonable interpretation based on our past experiences about potential scatterings. The S_{11} channel does not contain the nucleon as an s channel intermediate bound state, so the interaction is dominated by contact interaction and u channel nucleon exchange, which can

[17] The statistical errors are too small hence omitted here. See Table. 4 for details.

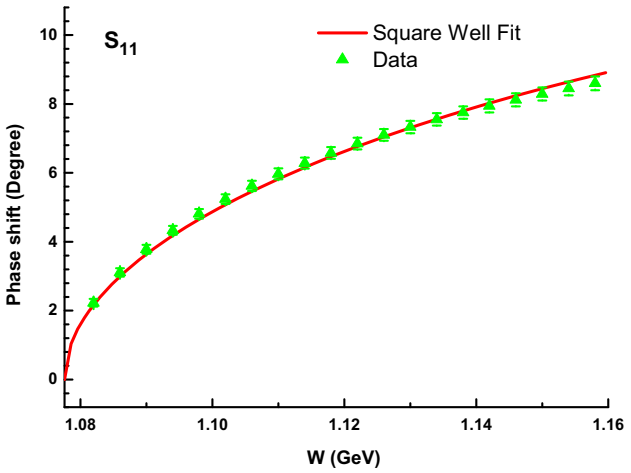

Fig. 9 The fit to the data with phase shift given by square well potential scatterings

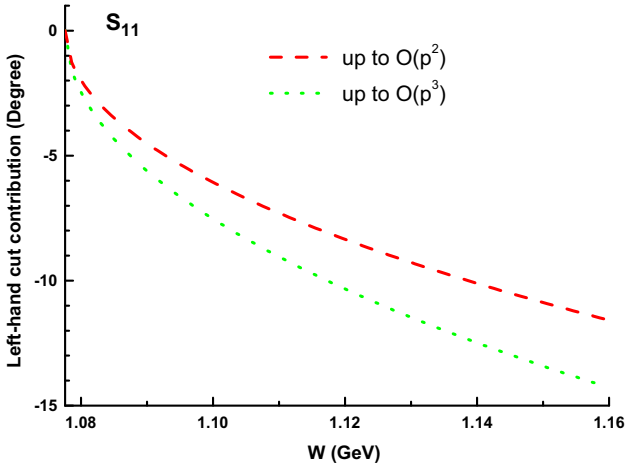

Fig. 10 The left-hand cut contributions in S_{11} channel up to $\mathcal{O}(p^2)$ and $\mathcal{O}(p^3)$. The cut-off parameters are determined by the $N^*(1440)$ shadow pole location, and the values of the low energy constants are taken from Table. 1 (Fit II) in Ref. [9]

be simulated as a potential. Typical potential scatterings can generate resonances below threshold; for example, we use the square-well potential as a toy model to show how this happens. The potential is

$$U(r) = 2\mu V(r) = \begin{cases} -2\mu V_0 & (r \le L), \\ 0 & (r > L), \end{cases} \tag{27}$$

where μ is the reduced mass of the pion and nucleon, r is the radial coordinate, $V_0 > 0$ and $L > 0$ are two parameters labeling the depth and range of the potential respectively. The textbook calculation of S- wave Schrödinger equation gives the phase shift, as a function of $3-$ momentum k in centre of mass frame:

$$\delta_{\rm sw}(k) = \arctan\left[\frac{k\tan k'L - k'\tan kL}{k' + k\tan(kL)\tan(k'L)}\right], \tag{28}$$

with $k' = (k^2 + 2\mu V_0)^{1/2}$. The fit to the data in S_{11} channel (20 data points) results in $L = 0.829$ fm and $V_0 = 144$ MeV, with fit quality $\chi^2_{\rm sw}/{\rm d.o.f} = 0.740$, see Fig. 9.

The poles are extracted via the equation $1 - i\tan\delta_{\rm sw}(k) = 0$, the nearest one of which locates at $k = -346i$ MeV as a deep virtual state, which in $\sqrt{s}$ plane turns out to be a "crazy resonance":[18]

$$\sqrt{s} = \sqrt{k^2+m^2} + \sqrt{k^2+M^2} \sim 0.872 - 0.316i \text{ GeV}. \tag{29}$$

Note that the deep virtual state suggested by the square well potential is already out of the non-relativistic energy region, but it still agrees with the result of PKU representation analyses (Eq. 26) qualitatively. Even though the square well potential calculation is only a toy model analysis, one expects that it may be helpful to reveal the correct physical picture that the "crazy resonance" is of potential scattering nature, generated from a not very strong but attractive potential. However, it should be warned that the hidden pole position in S_{11} channel is inside the circular left-hand cut ${\rm Re}(s)^2 + {\rm Im}(s)^2 = (M^2 - m^2)^2$, which, though only appears when the one loop contributions are under consideration, indicates that the one loop results may have critical impact on the hidden pole. One may even doubt that such a hidden pole is only a fake effect simulating the circular cut contribution, which are not presented at the moment. Nevertheless, as already discussed in Sect. 3.2, higher order calculations to the left-hand cut should not alter the qualitative picture presented here. This expectation is supported by the crucial calculation at $\mathcal{O}(p^3)$ level [38]. Briefly speaking, our $\mathcal{O}(p^3)$ preliminary result shows the hidden pole remains below threshold, since the left-hand cut contribution up to $\mathcal{O}(p^3)$ in S_{11} channel differs little from $\mathcal{O}(p^2)$, see Fig. 10.

4 Conclusions and outlook

In this work, we apply PKU representation, which separates the phase shifts into terms corresponding to different poles and branch cuts, to analyse processes of πN elastic scatterings. The contribution of background term, i.e. left-hand cut contribution, is deduced from tree amplitude derived in manifestly covariant BChPT. It is found that the left-hand cut in each S- or P- wave channel contributes negatively to the phase shift, in agreement with conventional wisdom.

Having estimated the left and right-hand cut contributions, it is found, particularly in P_{11} and S_{11} channels, the total con-

[18] The second pole given by square-well potential is at $2.28 - 1.06i$ GeV, which is too far away from the expected $N^*(1535)$ position.

tribution of the known poles and branch cuts are apparently insufficient to yield a satisfactory description of the experimental data. Thus certain significant positive contributions are required to compensate the discrepancies in those two channels.

In P_{11} wave, with the assistance of PKU representation, a kinematical near-threshold virtual state induced by the nucleon bound state pole is discovered, the location of which is found to be compatible with that calculated from perturbation theory. The discovery of that pole demonstrates the uncertainties from left-hand cut contributions extracted from the perturbation amplitudes is well under control in the framework of PKU representation. Further, the origin of such a virtual pole has not been discussed in the literature before.

Assuming that the S_{11} channel includes an extra hidden pole, we determine its position on the second Riemann sheet by fitting to phase shift data. It is found that the S_{11} channel may cache a pole lying well below the πN threshold, behaving as a so-called "crazy resonance". To reveal the existence of such a pole is completely novel.

There are still many follow-ups of this work to be done in future. For instance, the calculation of the left-hand cut integral could be extended to $\mathcal{O}(p^3)$ level, which is underway; methods based on crossing symmetry, e.g. Roskies relation or Roy-Steiner equations [6], may be incorporated into to get a cross-check on the determination of pole location in S_{11} channel. The physics related to such a novel resonance remains to be explored.

Acknowledgements We are grateful to one referee's useful suggestions and constructive remarks which are helpful in formulating the present version of this paper. This work is supported in part by National Nature Science Foundations of China (NSFC) under Contract Nos. 10925522, 11021092, by the Spanish Ministerio de Economía y Competitividad and the European Regional Development Fund, under contracts FIS2014-51948-C2-1-P, FIS2014-51948-C2-2-P, SEV-2014-0398 and by Generalitat Valenciana under contract PROMETEOII/2014/0068. DLY acknowledges the hospitality of the ITP of CAS where part of this work was done.

Funded by SCOAP[3].

Appendices

A Tree-level A, B functions

The expressions of the A, B functions can be found elsewhere, e.g., Refs. [8,9]. For completeness, we show the results as follows. At $\mathcal{O}(p^1)$ level

$$A_1^{1/2} = \frac{g^2 M}{F^2}, \tag{30}$$

$$B_1^{1/2} = \frac{1-g^2}{2F^2} - \frac{3M^2 g^2}{F^2(s-M^2)} - \frac{M^2 g^2}{F^2}\frac{1}{u-M^2}, \tag{31}$$

$$A_1^{3/2} = \frac{g^2 M}{F^2}, \tag{32}$$

$$B_1^{3/2} = -\frac{1-g^2}{2F^2} + \frac{2M^2 g^2}{F^2(u-M^2)}; \tag{33}$$

and for $\mathcal{O}(p^2)$

$$A_2^{1/2} = -\frac{4c_1 m^2}{F^2} + \frac{c_2(s-u)^2}{8M^2F^2} + \frac{c_3}{F^2}(2m^2-t) - \frac{c_4(s-u)}{F^2}, \tag{34}$$

$$B_2^{1/2} = \frac{4Mc_4}{F^2}, \tag{35}$$

$$A_2^{3/2} = -\frac{4c_1 m^2}{F^2} + \frac{c_2(s-u)^2}{8M^2F^2} + \frac{c_3}{F^2}(2m^2-t) + \frac{c_4(s-u)}{2F^2}, \tag{36}$$

$$B_2^{3/2} = -\frac{2Mc_4}{F^2}, \tag{37}$$

where the subscripts denote the chiral orders.

B Partial wave helicity amplitudes

In this section, we express the explicit expressions of πN partial wave amplitudes at tree level, which presents the left-hand cut structure clearly. To the best of our knowledge, these expressions have never been exhibited in previous literature. In what follows, we use the abbreviations: $R_m = M^2 - m^2$, $R_p = M^2 + m^2$, $c_L = (M^2 - m^2)^2/M^2$ and $c_R = M^2 + 2m^2$. The kinematic factor $\rho(s)$ is given by Eq. (4).

B.1 $\mathcal{O}(p^1)$ amplitudes

The $\mathcal{O}(p^1)$ partial wave helicity amplitudes are written as

$$T_{++}^{I,J} = \mathfrak{A}^{I,J} + \mathfrak{B}^{I,J} I_C^J(s), \tag{38}$$

$$T_{+-}^{I,J} = \frac{1}{\sqrt{s}}(\mathfrak{C}^{I,J} + \mathfrak{D}^{I,J} I_S^J(s)), \tag{39}$$

with definite isospin I and angular momentum J. In Eqs. (38) and (39), the $I_{C,S}$ functions corresponding to the u-channel nucleon exchange are singled out from the partial wave helicity amplitudes with the coefficients $\mathfrak{A}$, $\mathfrak{B}$, $\mathfrak{C}$ and $\mathfrak{D}$. The $I_{C,S}$ functions have the form of

$$I_C^{1/2}(s) = \int_{-1}^{1} \frac{1+z_s}{2(u-M^2)} dz_s = -\frac{2}{s^2\rho^4}\Big[\frac{M^2}{s}(s-c_L)\Big(\ln\frac{M^2}{s} + \ln\frac{s-c_L}{s-c_R}\Big) + s\rho^2\Big], \quad (40)$$

$$I_S^{1/2}(s) = \int_{-1}^{1} \frac{1-z_s}{2(u-M^2)} dz_s = \frac{2}{s^2\rho^4}\Big[(s-c_R)\Big(\ln\frac{M^2}{s} + \ln\frac{s-c_L}{s-c_R}\Big) + s\rho^2\Big], \quad (41)$$

for $J = 1/2$ and

$$I_C^{3/2}(s) = \int_{-1}^{1} \frac{(1+z_s)(3z_s-1)}{4(u-M^2)} dz_s = \frac{1}{s^5\rho^6}\Big\{2M^2(s-c_L)\big[2s(s-m^2) - M^2c_L - sc_R\big]\Big(\ln\frac{M^2}{s} + \ln\frac{s-c_L}{s-c_R}\Big) + s^2\rho^2(s^2 - 2m^2s - 5M^2c_L + 4M^2s)\Big\}, \quad (42)$$

$$I_S^{3/2}(s) = \int_{-1}^{1} \frac{(1-z_s)(3z_s+1)}{4(u-M^2)} dz_s = -\frac{1}{s^4\rho^6}\Big\{2(s-c_R)(s^2 + M^2s - 2m^2s - 2M^2c_L)\Big(\ln\frac{M^2}{s} + \ln\frac{s-c_L}{s-c_R}\Big) + s\rho^2\big[4(s-c_R)s - 2sm^2 + s^2 - M^2c_L\big]\Big\}, \quad (43)$$

for $J = 3/2$, where the Mandelstam variable u is given by

$$u(s, z_s) = R_p - \frac{s^2 - R_m^2}{2s} - \frac{(s-s_L)(s-s_R)}{2s} z_s. \quad (44)$$

The expressions of $\mathfrak{A}$, $\mathfrak{B}$, $\mathfrak{C}$ and $\mathfrak{D}$ in Eqs. (38) and (39) are as follows.

- $I = 1/2, J = 1/2$

$$\mathfrak{A}^{1/2,1/2} = \frac{s-R_p}{32F^2\pi} - \frac{g^2(s^2 - R_p s - 2m^2M^2)}{32F^2\pi(s-M^2)}, \quad (45)$$

$$\mathfrak{B}^{1/2,1/2} = -\frac{g^2M^2(s-R_p)}{32\pi F^2}, \quad (46)$$

$$\mathfrak{C}^{1/2,1/2} = \frac{M(s-R_m)}{32F^2\pi} - \frac{Mg^2(sc_R - M^2R_m)}{32F^2\pi(s-M^2)}, \quad (47)$$

$$\mathfrak{D}^{1/2,1/2} = -\frac{g^2M^3(s-R_m)}{32\pi F^2}. \quad (48)$$

- $I = 3/2, J = 1/2$

$$\mathfrak{A}^{3/2,1/2} = \frac{-(s-R_p) + g^2(s + 3M^2 - m^2)}{64F^2\pi}, \quad (49)$$

$$\mathfrak{B}^{3/2,1/2} = \frac{g^2M^2(s-R_p)}{16\pi F^2}, \quad (50)$$

$$\mathfrak{C}^{3/2,1/2} = \frac{M\big[-(s-R_m) + g^2(3s+R_m)\big]}{64\pi F^2}, \quad (51)$$

$$\mathfrak{D}^{3/2,1/2} = \frac{g^2M^3(s-R_m)}{16\pi F^2}. \quad (52)$$

- $I = 1/2, J = 3/2$

$$\mathfrak{A}^{1/2,3/2} = 0, \quad (53)$$

$$\mathfrak{B}^{1/2,3/2} = -\frac{g^2M^2(s-R_p)}{32\pi F^2}, \quad (54)$$

$$\mathfrak{C}^{1/2,3/2} = 0, \quad (55)$$

$$\mathfrak{D}^{1/2,3/2} = -\frac{g^2M^3(s-R_m)}{32\pi F^2}. \quad (56)$$

- $I = 3/2, J = 3/2$

$$\mathfrak{A}^{3/2,3/2} = 0, \quad (57)$$

$$\mathfrak{B}^{3/2,3/2} = \frac{g^2M^2(s-R_p)}{16\pi F^2}, \quad (58)$$

$$\mathfrak{C}^{3/2,3/2} = 0, \quad (59)$$

$$\mathfrak{D}^{3/2,3/2} = \frac{g^2M^3(s-R_m)}{16\pi F^2}. \quad (60)$$

B.2 $\mathcal{O}(p^2)$ amplitudes

The helicity amplitudes of $\mathcal{O}(p^2)$ with $J = 1/2$ are

$$T_{++}^{I=1/2,J=1/2} = \frac{c_2 I_{C2}^{1/2} - 8M^2\{4c_1m^2 - c_3 I_{Ct}^{1/2} + c_4[I_{C1}^{1/2} - 2(s-R_p)]\}}{128\pi MF^2}, \quad (61)$$

$$T_{+-}^{I=1/2,J=1/2} = \frac{32c_4M^4(s-R_m) + (s+R_m)[c_2 I_{S2}^{1/2} + 8M^2(c_3 I_{St}^{1/2} - c_4 I_{S1}^{1/2} - 4c_1m^2)]}{256\pi M^2F^2\sqrt{s}}, \quad (62)$$

$$T_{++}^{I=3/2,J=1/2} = \frac{c_2 I_{C2}^{1/2} + 4M^2\{-8c_1m^2 + 2c_3 I_{Ct}^{1/2} + c_4[I_{C1}^{1/2} - 2(s-R_p)]\}}{128\pi MF^2}, \quad (63)$$

$$T_{+-}^{I=3/2,J=1/2} = \frac{-16c_4M^4(s-R_m) + (s+R_m)[c_2 I_{S2}^{1/2} + 4M^2(2c_3 I_{St}^{1/2} + c_4 I_{S1}^{1/2} - 8c_1m^2)]}{256\pi M^2F^2\sqrt{s}}, \quad (64)$$

where the $I_{\ldots}^{1/2}$ are some partial-wave integrals, specifically,

$$I_{C1}^{1/2}=\int_{-1}^{1}\frac{z_s+1}{2}\big[s-u(s,z_s)\big]=-\frac{R_m^2}{3s}-\frac{4}{3}R_p+\frac{5}{3}s, \tag{65}$$

$$I_{C2}^{1/2}=\int_{-1}^{1}\frac{z_s+1}{2}\big[s-u(s,z_s)\big]^2=\frac{R_m^4}{6s^2}+\frac{2R_m^2R_p}{3s}+(m^4+6m^2M^2+M^4)-\frac{14}{3}R_ps+\frac{17s^2}{6}, \tag{66}$$

$$I_{Ct}^{1/2}=\int_{-1}^{1}\frac{z_s+1}{2}\big[2m^2-t(s,z_s)\big]=\frac{R_m^2}{3s}+\frac{2}{3}(2m^2-M^2)+\frac{s}{3}, \tag{67}$$

and

$$I_{S1}^{1/2}=\int_{-1}^{1}\frac{z_s-1}{2}\big[s-u(s,z_s)\big]=-\frac{2R_m^2}{3s}-\frac{2}{3}R_p+\frac{4}{3}s, \tag{68}$$

$$I_{S2}^{1/2}=\int_{-1}^{1}\frac{z_s-1}{2}\big[s-u(s,z_s)\big]^2=\frac{R_m^4}{2s^2}+\frac{2R_m^2R_p}{3s}-\frac{3m^4-14m^2M^2+3M^4}{3}-2R_ps+\frac{11s^2}{6}, \tag{69}$$

$$I_{St}^{1/2}=\int_{-1}^{1}\frac{z_s-1}{2}\big[2m^2-t(s,z_s)\big]=\frac{2R_m^2}{3s}+\frac{2}{3}(m^2-2M^2)+\frac{2s}{3}, \tag{70}$$

with

$$t(s,z_s)=2m^2-\frac{s^2-R_m^2}{2s}-\frac{(s-s_L)(s-s_R)}{2s}z_s. \tag{71}$$

For the case of $J=3/2$,

$$T_{++}^{I=1/2,J=3/2}=\frac{c_2I_{C2}^{3/2}+8M^2(c_3I_{Ct}^{3/2}-c_4I_{C1}^{3/2})}{128\pi MF^2}, \tag{72}$$

$$T_{+-}^{I=1/2,J=3/2}=\frac{(s+R_m)\big[c_2I_{S2}^{3/2}+8M^2(c_3I_{St}^{3/2}-c_4I_{S1}^{3/2})\big]}{256\pi M^2F^2\sqrt{s}}, \tag{73}$$

$$T_{++}^{I=3/2,J=3/2}=\frac{c_2I_{C2}^{3/2}+4M^2(2c_3I_{Ct}^{3/2}+c_4I_{C1}^{3/2})}{128\pi MF^2}, \tag{74}$$

$$T_{+-}^{I=3/2,J=3/2}=\frac{(s+R_m)\big[c_2I_{S2}^{3/2}+4M^2(2c_3I_{St}^{3/2}+c_4I_{S1}^{3/2})\big]}{256\pi M^2F^2\sqrt{s}}, \tag{75}$$

with

$$I_{C1}^{3/2}=\int_{-1}^{1}\frac{(z_s+1)(3z_s-1)}{4}\big[s-u(s,z_s)\big]=\frac{-2m^2(s+M^2)+m^4+(s-M^2)^2}{6s}, \tag{76}$$

$$I_{C2}^{3/2}=\int_{-1}^{1}\frac{(z_s+1)(3z_s-1)}{4}\big[s-u(s,z_s)\big]^2=\frac{2(s-s_L)(s-s_R)(4s^2-3R_ps-R_m^2)}{15s^2}, \tag{77}$$

$$I_{Ct}^{3/2}=\int_{-1}^{1}\frac{(z_s+1)(3z_s-1)}{4}\big[2m^2-t(s,z_s)\big]=-\frac{-2m^2(s+M^2)+m^4+R_m^2}{6s}, \tag{78}$$

and

$$I_{S1}^{3/2}=\int_{-1}^{1}\frac{(z_s-1)(3z_s+1)}{4}\big[s-u(s,z_s)\big]=\frac{-2m^2(s+M^2)+m^4+(s-M^2)^2}{6s}, \tag{79}$$

$$I_{S2}^{3/2}=\int_{-1}^{1}\frac{(z_s-1)(3z_s+1)}{4}\big[s-u(s,z_s)\big]^2=\frac{(s-s_L)(s-s_R)(7s^2-4R_ps-3R_m^2)}{15s^2}, \tag{80}$$

$$I_{St}^{3/2}=\int_{-1}^{1}\frac{(z_s-1)(3z_s+1)}{4}\big[2m^2-t(s,z_s)\big]=-\frac{-2m^2(s+M^2)+m^4+(s-M^2)^2}{6s}. \tag{81}$$

C Examinations on the uncertainties of left-hand cut integrals

C.1 Varying low energy constants

In this section we show that the variation of $\mathcal{O}(p^2)$ low energy constants c_i in Eq. (7) has little impact on the results of PKU representation analyses. Three sets of c_i values are employed: set 1 is the result of K-matrix fit to the phase shift data in this paper, see Sect. 3; set 2 is from the K-matrix fit to the phase shift data at $\mathcal{O}(p^3)$ level, see Table. 1 (Fit II) in Ref. [9]; set 3 is the values that are given by the fit to the subthreshold parameters from Roy-Stainer analyses at $\mathcal{O}(p^2)$ level, see Table. 1 in Ref. [34]. From Fig. 11 it is clear that the left-hand cut contributions of different c_i values are quite close to each other, hence the main results of this paper are irrelevant to different c_i determinations.

C.2 Changing integration cut-off s_c

In what follows we investigate the effect of the variations of the cut-off s_c in Eq. (17): s_c ranges from $-0.08\,\mathrm{GeV}^2$ to $-\infty$, see Fig. 12. It is found that the cut-off parameter is actually of some numerical importance, but the qualitative picture never changes. Besides, the missing contributions in S_{11} and P_{11} channels can never be blotted out by changing s_c.

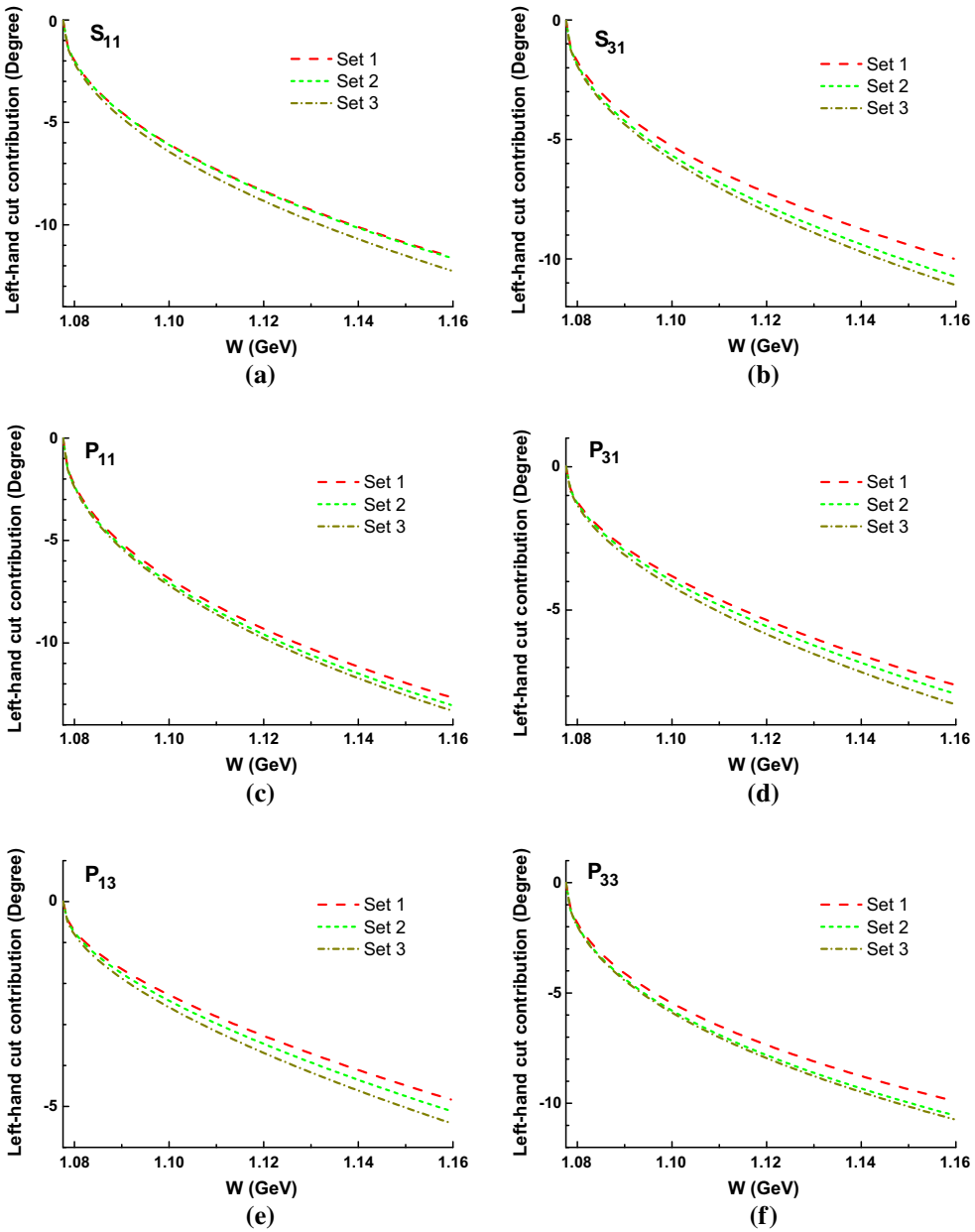

Fig. 11 Left-hand cut contributions with different values of low energy constants c_i

In S_{11} channel, it is found that the extra pole stays below threshold when s_c changes, see Table. 4.

On the other hand, the residue at the hidden pole is also non-negligible compared to that of $N^*(1535)$, see Table. 5.

Finally, one may wonder what happens if a narrower interval of the left-hand cut integral, i.e. $s_c > -0.08\,\text{GeV}^2$, is chosen. Actually, using $s_c = 0.32\,\text{GeV}^2$ determined by $\Delta(1232)$ pole location, one obtains rather small left-hand cut contributions and subsequently very poor fit in each channel, such that in S_{31}, P_{31}, P_{13} and P_{33} channels significant negative phase shift contributions are needed to match the data. This is ridiculous since the only source of negative contribution (except those coming from left-hand cut) is the bound state contribution, and bound states are physical and should be observed in nature. The conclusion is that one needs negative phase shift contribution from the left-hand cut integral beyond perturbation region. To say the least, even though choosing $s_c = 0.32\,\text{GeV}^2$, the existence of those extra states are still for sure, since for all possible s_c values the left-hand cut can never give a significant positive contribution to match the data.

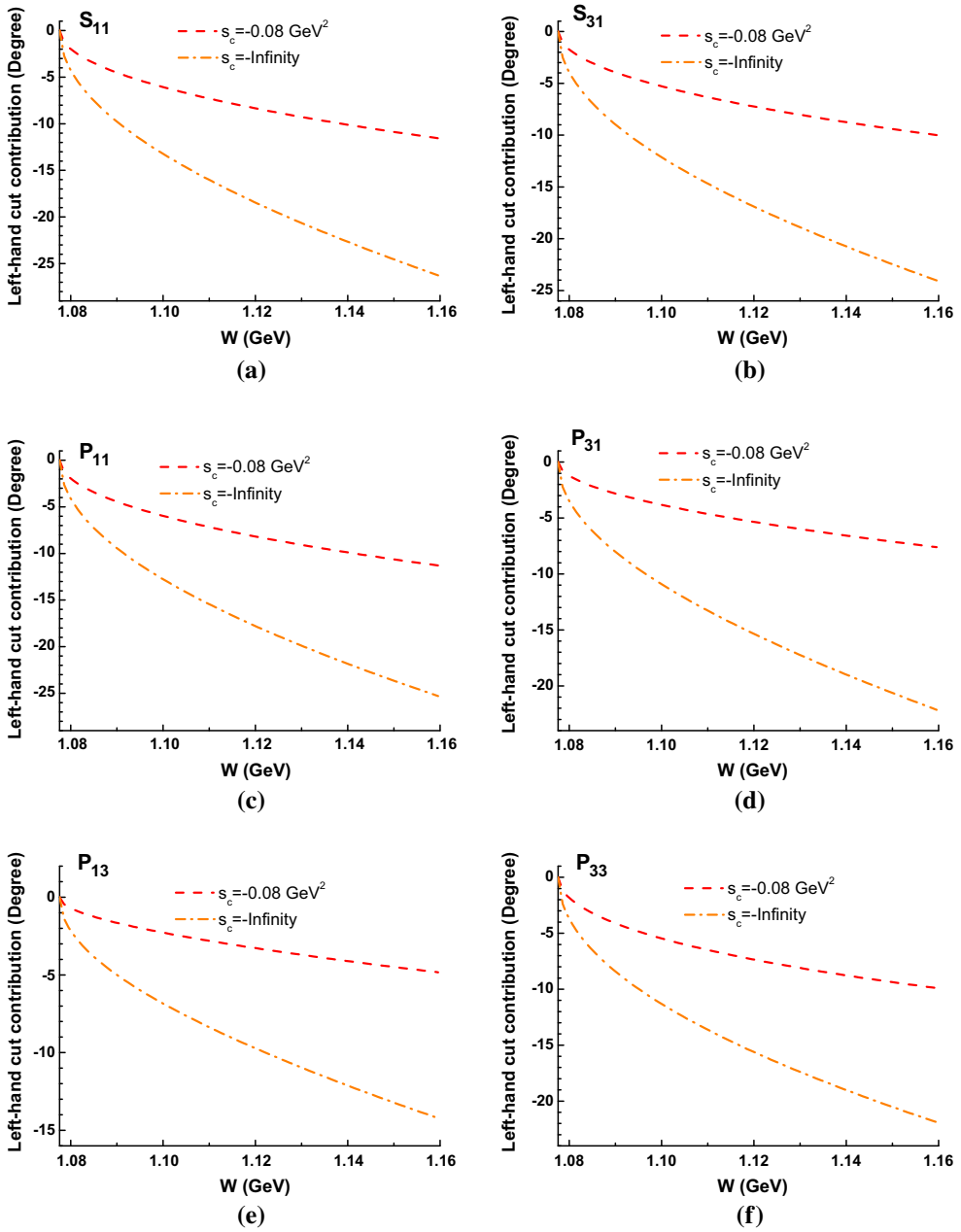

Fig. 12 Left-hand cut contributions given by PKU representation under different cut-off values

Table 4 The S_{11} hidden pole fit with different choices of s_c

s_c (GeV^2)	Pole position (GeV)	Fit quality χ^2/d.o.f	Statistical error (MeV)
-0.08	$0.808-0.055i$	0.109	$8.2-18.5i$
-1.00	$0.822-0.139i$	0.076	$0.1-14.8i$
-9.00	$0.883-0.195i$	0.034	$0.7-10.1i$
∞	$0.914-0.205i$	0.018	$2.1-8.1i$

Table 5 The residues of the S_{11} hidden resonance and $N^*(1535)$ Shadow pole (in units of GeV^2)

s_c	Residue of the hidden state	Residue of $N^*(1535)$ shadow pole
-0.08	$(0.422+0.107i)^2$	$(0.229+0.029i)^2$
-1.00	$(0.449+0.124i)^2$	$(0.228+0.038i)^2$
-9.00	$(0.460+0.173i)^2$	$(0.223+0.059i)^2$
$-\infty$	$(0.456+0.199i)^2$	$(0.218+0.074i)^2$

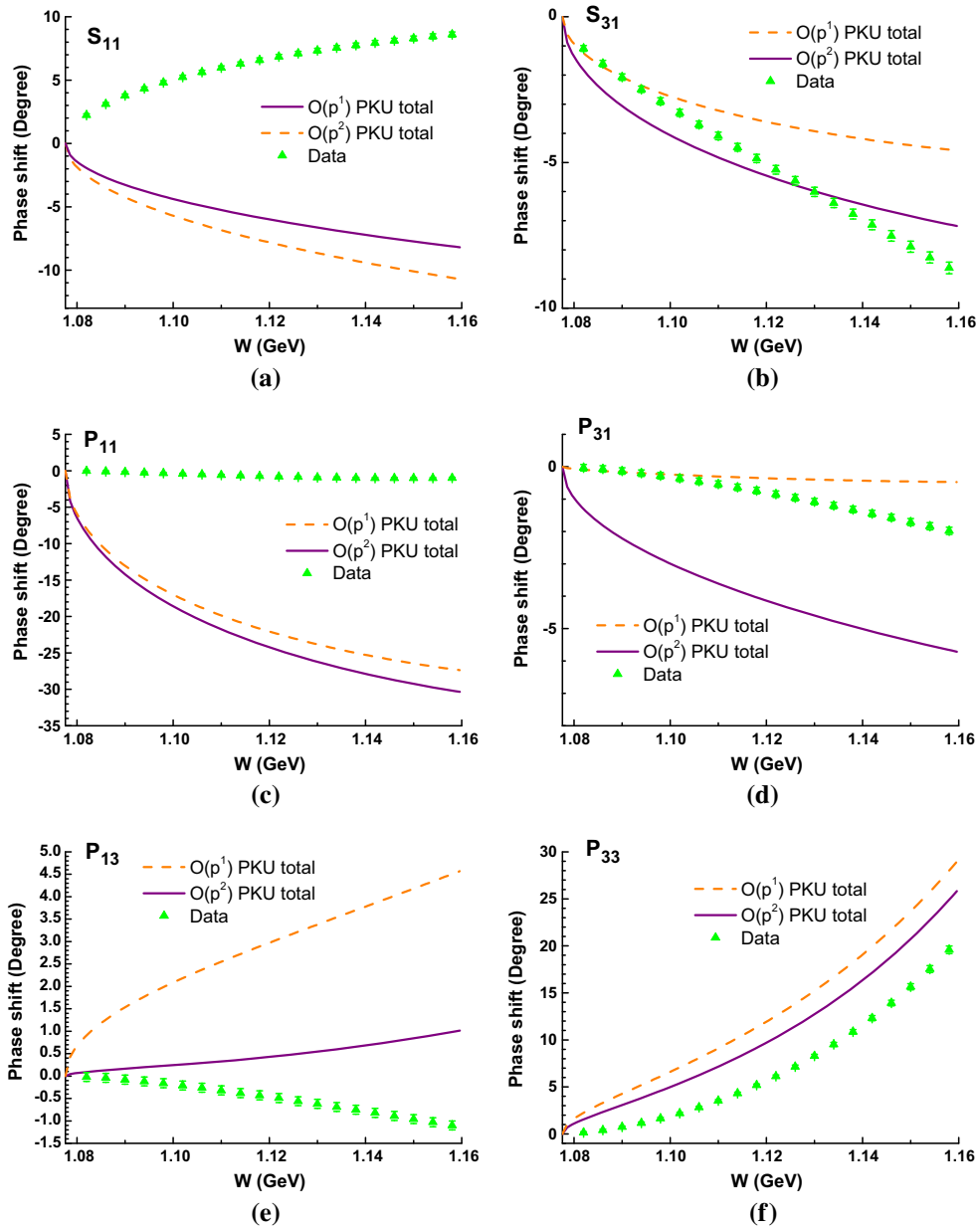

Fig. 13 Comparison of PKU representation analyses between $\mathcal{O}(p^1)$ and $\mathcal{O}(p^2)$

C.3 Truncating chiral orders: $\mathcal{O}(p^1)$ versus $\mathcal{O}(p^2)$

The phase shifts from both $\mathcal{O}(p^1)$ and $\mathcal{O}(p^2)$ chiral amplitudes are plotted in Fig. 13, where the cut-off parameter of the background integral is taken as $-0.08\,\mathrm{GeV}^2$. We present the different estimation of the phase shifts here, for the purpose of comparing the perturbative calculations at different orders. It can be seen that the difference of phase shift results between $\mathcal{O}(p^1)$ and $\mathcal{O}(p^2)$ are only at the order of a few degrees, and at $\mathcal{O}(p^1)$ the S_{11} and P_{11} channels also contain significant disagreements between the known poles plus cut and the data. In general, the qualitative conclusions remain unchanged when the chiral order changes.

D Checking the S matrix zero in P_{11} channel with subthreshold expansion

Here we use the subthreshold parameters given in Ref. [13] to search for the near-threshold S matrix zero in P_{11} channel, for the sake of comparison to the perturbation result in Fig. 7. We take the A, B functions in the form of Eq. (3.32), Eq. (3.33) and Eq. (3.34), and the values of the constants in Table. 4 (the

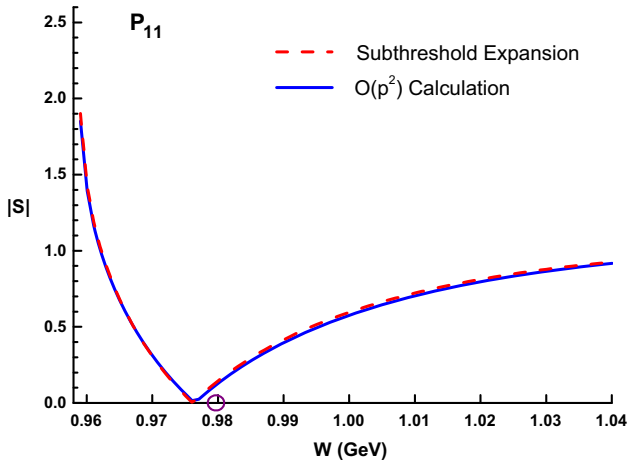

Fig. 14 The absolute value of S matrix in P_{11} channel. The circle marks the location of the P_{11} virtual state given by fit using $s_c = -9\ \mathrm{GeV}^2$

RS results) in Ref. [13]; then we do partial wave projection using Eqs. (13), (14) and (15) in this paper to extract the P_{11} amplitude. As shown in Fig. 14, the subthreshold expansion gives almost the same result as the $\mathcal{O}(p^2)$ calculation.

References

1. B.H. Bransden, R.G. Moorhouse, *The Pion-Nucleon System* (Princeton University Press, Princeton, 1973)
2. G. Höhler, L.B. Vol, *9b2. edited by H. Schopper* (Springer, Berlin, 1983)
3. T. Becher, H. Leutwyler, JHEP **0106**, 017 (2001)
4. A. Gasparyan, M.F.M. Lutz, Nucl. Phys. A **848**, 126 (2010)
5. J.M. Alarcon, J. Martin Camalich, J.A. Oller, L. Alvarez-Ruso, Phys. Rev. C **83**, 055205 (2011)
6. C. Ditsche, M. Hoferichter, B. Kubis, U.-G. Meißner, JHEP **1206**, 043 (2012)
7. J.M. Alarcon, J. Martin Camalich, J.A. Oller, Phys. Rev. D **85**, 051503 (2012)
8. J.M. Alarcon, J. Martin Camalich, J.A. Oller, Ann. Phys. **336**, 413 (2013)
9. Y.H. Chen, D.L. Yao, H.Q. Zheng, Phys. Rev. D **87**, 054019 (2013)
10. M. Hoferichter, J. Ruiz de Elvira, B. Kubis, U.-G. Meißner, Phys. Rev. Lett. **115**, 092301 (2015)
11. D. Siemens, V. Bernard, E. Epelbaum, A.M. Gasparyan, H. Krebs, U.-G. Meißner, Phys. Rev. C **94**, 014620 (2016)
12. D.L. Yao, D. Siemens, V. Bernard, E. Epelbaum, A.M. Gasparyan, J. Gegelia, H. Krebs, U.-G. Meißner, JHEP **1605**, 038 (2016)
13. M. Hoferichter, J. Ruiz de Elvira, B. Kubis, U.-G. Meißner, Phys. Rept. **625**, 1 (2016)
14. N. Kaiser, P.B. Siegel, W. Weise, Phys. Lett. B **362**, 23 (1995)
15. J. Nieves, E. Ruiz Arriola, Phys. Rev. D **64**, 116008 (2001)
16. O. Krehl, C. Hanhart, S. Krewald, J. Speth, Phys. Rev. C **62**, 025207 (2000)
17. R.A. Arndt, J.M. Ford, L.D. Roper, Phys. Rev. D **32**, 1085 (1985)
18. S. Ceci, M. Doring, C. Hanhart, S. Krewald, U.-G. Meißner, A. Svarc, Phys. Rev. C **84**, 015205 (2011)
19. Z. Xiao, H.Q. Zheng, Nucl. Phys. A **695**, 273 (2001)
20. J. He, Z. Xiao and H. Q. Zheng, Phys. Lett. B **536**, 59 (2002). Erratum: [Phys. Lett. B **549**, 362 (2002)]
21. H.Q. Zheng, Z.Y. Zhou, G.Y. Qin, Z. Xiao, J.J. Wang, N. Wu, Nucl. Phys. A **733**, 235 (2004)
22. Z.Y. Zhou, G.Y. Qin, P. Zhang, Z. Xiao, H.Q. Zheng, N. Wu, JHEP **0502**, 043 (2005)
23. Z.Y. Zhou, H.Q. Zheng, Nucl. Phys. A **775**, 212 (2006)
24. Z. Xiao, H.Q. Zheng, Commun. Theor. Phys. **48**, 685 (2007)
25. N. Hu, Phys. Rev. **74**, 131 (1948)
26. T. Regge, Nuovo Cim. **8**, 671 (1958)
27. G.Y. Qin, W.Z. Deng, Z. Xiao, H.Q. Zheng, Phys. Lett. B **542**, 89 (2002)
28. V. Bernard, N. Kaiser, U.-G. Meißner, Int. J. Mod. Phys. E **4**, 193 (1995)
29. N. Fettes, U.-G. Meißner, M. Mojzis and S. Steininger, Annals Phys. **283**, 273 (2000). Erratum: [Annals Phys. **288**, 249 (2001)]
30. S.W. MacDowell, Phys. Rev. **116**, 774 (1959)
31. J. Kennedy, T.D. Spearman, Phys. Rev. **126**, 1596 (1961)
32. A.V. Anisovich, R. Beck, E. Klempt, V.A. Nikonov, A.V. Sarantsev, U. Thoma, Eur. Phys. J. A **48**, 15 (2012)
33. C. Patrignani et al. [Particle Data Group], Chin. Phys. C **40**(10), 100001 (2016)
34. D. Siemens et al., Phys. Lett. B **770**, 27 (2017)
35. Computer code SAID, online program at http://gwdac.phys.gwu.edu/ (solution WI08), and R. A. Arndt et al., Phys. Rev. C **74**, 045205 (2006) (solution SM01)
36. D. Morgan, Nucl. Phys. A **543**, 632 (1992)
37. V.I. Kukulin, V.M. Krasnopol'sky, J. Horáček, *Theory of Resonances: Principles and Applications* (Kluwer Academic Publisher, Dordrecht, 1989)
38. Y.F. Wang, D.L. Yao, H.Q. Zheng, in preparation